

Weak quantization of noninteracting topological Anderson insulatorDinhDuy Vu  and Sankar Das Sarma*Condensed Matter Theory Center and Joint Quantum Institute,**Department of Physics, University of Maryland, College Park, Maryland 20742, USA* (Received 5 May 2022; revised 19 July 2022; accepted 26 September 2022; published 6 October 2022)

We study the transition between the two-dimensional topological insulator (TI) featuring quantized edge conductance and the trivial Anderson insulator induced by strong disorder. We discover a distinct scaling behavior of the TI near the phase transition where the longitudinal conductance approaches the quantized value by a power law with system size, instead of an exponential law in a clean TI. This region is thus called the weak quantization topological insulator. By using the self-consistent Born approximation, we associate the emergence of the weak quantization with the imaginary part of the effective self-energy acquiring a finite value at strong disorder. We use our analytical theory, supported by direct numerical simulations, to study the effect of disorder range on the topological Anderson insulator. Interestingly, while this phase is quite generic for uncorrelated or short-range disorder, it is strongly suppressed by long-range disorder, perhaps explaining why it has not been seen in solid state systems.

DOI: [10.1103/PhysRevB.106.134201](https://doi.org/10.1103/PhysRevB.106.134201)**I. INTRODUCTION**

Noninteracting topological phases are interesting not only from theoretical perspectives but also for potential applications. Because of the nonlocal topological characteristics, the most important signature of these phases is the anomalous boundary metallic mode robust to perturbative deformations of the Hamiltonian. In this paper, we focus on two-dimensional (2D) topological systems featuring robust conducting edge modes [1–7]. A paradigm of this class, and probably the most experimentally viable, is the quantum spin Hall insulator induced by the spin-orbit coupling and band inversion [8–13]. Such nontrivial topological insulators (TIs) manifest an odd number of conducting helical modes at the boundary and a stable quantized conductance against small parameter changes. Recently, an anomalous quantum Hall effect where chiral modes can exist without an external field has also been reported [14–16]. In all these experiments, quantized conductance is the key evidence to confirm the nontrivial topology.

The intuition behind the stability of the anomalous edge states can be explained as follows. In a clean topological system, electrons at one edge can only move in one direction (per each time-reversal partner) so backscattering is absent and the current flows around the defect [17]. As disorder becomes sufficiently strong, bulk parameters can be renormalized, driving the system to a different topological phase [18–32]. An interesting case is when the renormalized Hamiltonian itself supports nontrivial topology with robust boundary modes while the original clean system is trivial [20–22,24–27,30–34], the so-called topological Anderson insulator (TAI) phase. This phenomenon can also be studied in one-dimensional systems [35–38] and has been observed experimentally in atomic and optical systems [39], even though the topology

here is characterized through a bulk index rather than the associated gapless boundary mode. The quantization plateau should not survive to an arbitrarily large disorder strength, with the bulk eventually becoming the exponentially localized Anderson insulator (AI) with trivial topology and thus zero edge conductance. While early works numerically demonstrated a “levitation and pair annihilation” mechanism for the suppression of edge conductance [40,41], an intuitive physical picture is provided through a percolation process. Conducting bands, in the presence of disorder, generically develop tails of exponentially localized states that eventually overlap with the bulk gap [24,42]. These localized bulk “islands” become connected if the disorder landscape is correlated and form a percolating network, effectively acting as a passage for the two edge modes to percolate into the bulk and destroy the quantization plateau through an effective edge-edge coupling [43,44]. In comparison with the pristine system, the bulk density of state at the energy gap is exactly zero, so the edge-edge hybridization can only happen through tunneling across the vacuum bulk, which is exponentially suppressed with the distance.

In this paper, we study the transition regime between TI and AI with increasing disorder strength, focusing on the quantization plateau (and its eventual disappearance) in the two-terminal longitudinal conductance. We first numerically show that near the TI-AI phase boundary, the scaling of the conductance quantization error $(1 - G)$ with the system size is slower than any exponential laws usually observed in clean TIs. We refer to this region as the weak quantization topological insulator (WQTI), while reserving the TI nomenclature for a regime with exponentially fast quantization. This change of the scaling law distinguishes TI and WQTI. In the following, we show that this transition is the manifestation of the second-order transition of the imaginary part of the

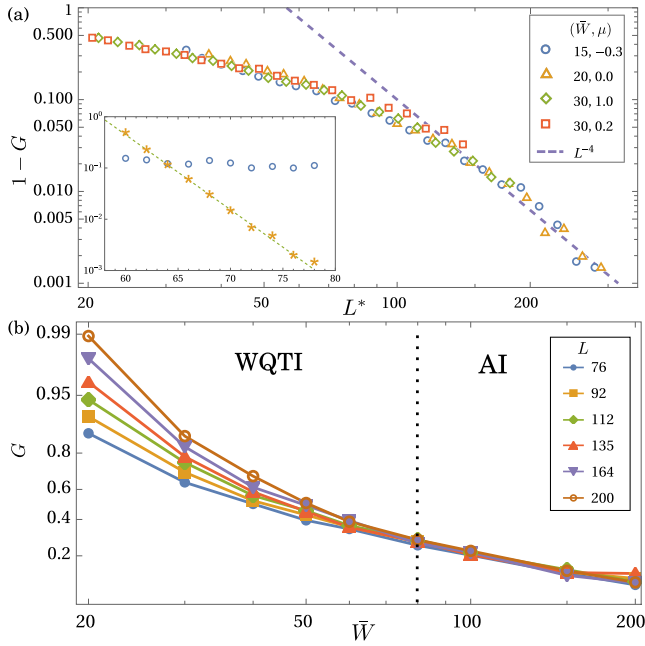


FIG. 1. (a) The quantization error $1 - G$ with the rescaled size L^* so that $1 - G$ at different parameters collapses into a single function with an asymptote L^{-4} . The inset shows the finite-size scaling of quantization error but in a log-linear graph, distinguishing the exponential decay for $W = 10$, $\mu = 0.5$ (yellow asterisks) from the polynomial decay for $W = 15$, $\mu = -0.3$ (blue circles). (b) The scaling of the conductance at $\mu = 0$ across the WQTI-AI transition. The vertical axis is plotted by the scale $\ln[y/(1-y)]$ to show both the limits near zero and one. The lattice parameters for the simulation are identical to Fig. 2(b).

self-energy acquiring a nonzero value for sufficiently strong disorder [see Fig. 2 and Fig. S2(a) of the Supplemental Material (SM) [45]].

Here, we describe how the WQTI fits into other phase classification schemes in the present literature. In terms of topological classification, WQTI and TI belong to the same phase and should exhibit perfect quantized conductance in the thermodynamic limit. However, for finite systems, TI (WQTI) would manifest robust (fragile) quantization, which has implications for experiments. This motivates our separation of WQTI from the TI phase based on the scaling behavior. We note that TAI refers to the disorder-induced quantized conductance phase starting from the pristine limit with no metallic edge modes, either because the bare (before the disorder-induced renormalization) mass is positive or the bare chemical potential lies outside the bulk gap. Therefore, TAI may overlap with either TI or WQTI depending on details.

A key distinguishing feature of our work compared with earlier works reporting similar numerical evidence is the development of an analytical framework that theoretically establishes the fragile power-law behavior of the WQTI phase. Furthermore, we predict the emergence of TI, WQTI, and AI phases based entirely on our analytical theory, obtaining excellent agreement with the exact numerical results. To demonstrate the predictive power of our theory, we study the effect of disorder range on the TAI region (with no

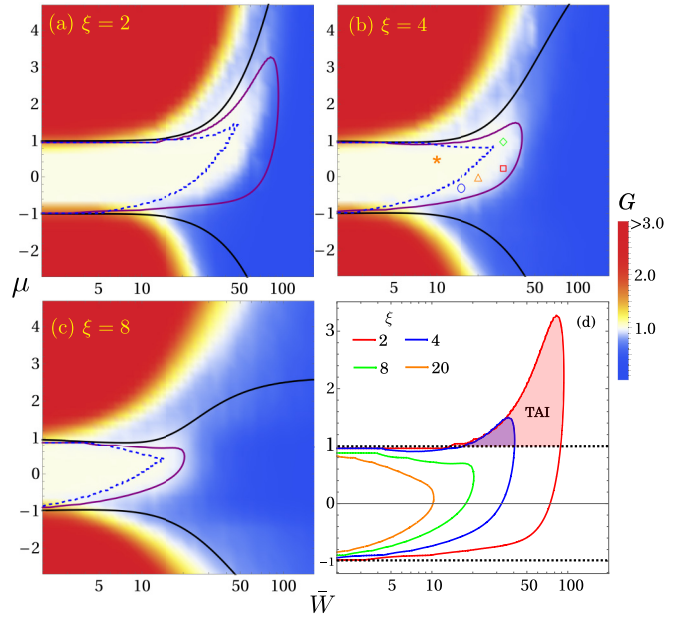


FIG. 2. (a)–(c) Longitudinal conductance with increasing disorder correlation lengths. For the specifications of the lattice, the width is $200a$, the length is $400a$, $m = -1$, $\alpha = 16$, $\beta = 100$, $\gamma = 48$. Points marked in (b) correspond to Fig. 1(a). The black lines show the renormalized energy gap $\bar{\mu} = \pm \bar{m}$, the purple lines are the $\Xi = 2$ isolines in Eq. (2), and the dashed blue lines are the boundary of the $\text{Im } \Sigma_0 = 0$ region. (d) The $\Xi = 2$ isolines (solid lines) at different correlation lengths. The dotted lines mark the energy gap in the pristine limit. Accordingly, the TAI phase (shaded region beyond the dotted lines) only exists for $\xi = 2$ and 4.

quantized-conductance clean analog). Both our analytic theory and numerical simulation show a progressive suppression of the quantization plateau as the disorder range increases. Again, this has been reported based on numerical simulations before [43,44], but our analytical model provides deep insight into the underlying physics. The main text of this paper is devoted to the on-site disorder, so, with no loss of generality, we only work on one spin sector of the Hamiltonian, leaving the other time-reversal partner implicit.

II. THEORY

We start with a clean Chern insulator Hamiltonian that preserves the translational symmetry,

$$H_0(k_x, k_y) = \alpha(k_x \sigma_x - k_y \sigma_y) + (m + \beta k^2) \sigma_z + \gamma k^2 \sigma_0. \quad (1)$$

The tunable chemical potential is μ . We perform the numerical simulation on a square lattice with the lattice constant a , using a discretized version of Eq. (1). The parameters α , β , γ when accompanied by an appropriate power of the lattice constant give the unit of energy, i.e., α/a , β/a^2 , and γ/a^2 have the same dimension as the mass m . Therefore, throughout this paper, we fix $a = 1$ and provide the value for α , β , γ with the length scale a implied. To reproduce the effect of quenched impurities, we introduce random disorder at each site whose strength is chosen independently from a uniform distribution $[-W/2, W/2]$. Each impurity interacts with electrons via a

Gaussian interaction, resulting in the disorder potential being long-range correlated $\langle u(\mathbf{r})u(\mathbf{r}') \rangle \sim e^{-(\mathbf{r}-\mathbf{r}')^2/2\xi^2}$ [45] ($\langle \cdot \rangle$ denotes averaging over disorder configurations.) The disordered Hamiltonian is thus $H_0 + u(\mathbf{r})\sigma_0$ with σ_0 reflecting the on-site disorder (other types of disorder differing by the accompanying matrix are studied in the SM [45]). Because of the finite correlation length, W, α are rescaled by ξ^{-1} and β, γ by ξ^{-2} [45]. For this reason, we use the rescaled disorder strength $\bar{W} = W/\xi$ instead of the absolute value in all the figures. The longitudinal conductance G is computed exactly using the Landauer-Büttiker formalism [17,46] and implemented numerically using the KWANT package [47]. We average over up to 700 disorder configurations to ensure convergence and present the conductance in the unit of e^2/h so that the ideal TI quantized conductance is unity.

From the theoretical perspective, we can average the Green's function over disorder configurations to obtain an effective theory with recovered translational symmetry, i.e., $G = \langle [\mu - H_0 - u(\mathbf{r})\sigma_0]^{-1} \rangle = (\mu - H_0 - \Sigma)^{-1}$. This self-energy Σ is a matrix $\Sigma = \Sigma_0\sigma_0 + \Sigma_z\sigma_z$ (by symmetry reasoning there are no $\sigma_{x,y}$ terms). If we only consider noncrossing diagrams (i.e., the self-consistent Born approximation), the self-energy can be written as an integral equation [45]. Due to renormalization by the self-energy, the renormalized mass $\bar{m} = m + \text{Re} \Sigma_z$ and chemical potential $\bar{\mu} = \mu - \text{Re} \Sigma_0$ define a new energy gap by the condition $\bar{m} < 0$ and $|\bar{\mu}| < |\bar{m}|$. However, as shown in the numerical results (Fig. 2), the boundary generated from the gap-opening condition, defined only by the real parts of the self-energy, does not enclose the TI region but in fact extends far beyond. Thus, a theory based only on mass and chemical potential renormalization, described by the real part of the self-energy, is incomplete. We take into account the imaginary part of the self-energy analytically and obtain the boundary enclosing the numerically simulated quantization plateau, thus providing a complete and correct theory.

We first provide a preliminary argument. The gapless boundary modes inherit the imaginary term from the bulk which can be regarded as the incoherent broadening of the edge excitation. As such, the edge current can disperse into the bulk where it might hybridize with the current leaking from the opposite edge and mutually exchange momentum. This effective coupling between the two chiral edges, arising from the impurity-scattering-induced imaginary self-energy, leads to the quantization error and eventually the suppression of the conducting edge modes. This is the physical mechanism driving the TI-WQTI-AI transition with increasing charge disorder. Formally, when the two edge states hybridize, the quantization error in the longitudinal conductance is proportional to hybridization probability. In the SM [45], we evaluate this probability as $\sim F(\Delta E/\Gamma)L^{-4}$. Here, F is a function, ΔE is the energy separation between the renormalized chemical potential and the edges of the renormalized bulk gap, Γ is the energy level broadening, and L is the interedge separation. The level broadening may arise from either $\text{Im} \Sigma_0$ or $\text{Im} \Sigma_z$, but the edge states are the eigenvectors of σ_x , so only the former can contribute to the L^{-4} scaling. We thus identify $\Gamma = \text{Im} \Sigma_0$. From this dimensional scaling analysis, if the imaginary part of the self-energy is nonzero, $1 - G$ should

scale as L^{-4} ; and, if it is zero, the quantization converges exponentially because the two edges can only interact through tunneling which is suppressed exponentially in the absence of level broadening.

To quantify this physics, we numerically compute the quantization error $1 - G$ while changing the system width (the ratio length/width is fixed at 2). For points with nonzero $\text{Im} \Sigma_0$ [see Fig. 2(b)], $1 - G$ decreases with increasing system size by a subexponential scaling law as shown in the log-log plot in Fig. 1(a). After rescaling L , there emerges a one-parameter scaling function $\beta = d \ln(1 - G)/d \ln L$ that approaches -4 for G sufficiently close to unity, consistent with our analytical picture of the interedge hybridization through the bulk leakage. Because of this power-law scaling of the quantization error, we refer to this phase as the WQTI. Compared with the pristine TI, we compute the quantization error for a point with vanishing $\text{Im} \Sigma_0$ (but a finite strength of disorder) which, as shown in the inset of Fig. 1(a), has a clear exponential scaling. This comparison establishes that the disorder-induced TI-WQTI transition is driven by the imaginary part of the self-energy acquiring a finite value beyond a critical point, resulting in the edge localization length diverging across the phase transition (and thus hybridizing in the WQTI phase). While earlier works numerically demonstrated the strong finite-size effect observed in the presence of strong disorder [24,33,48], we quantify this behavior by providing the one-parameter scaling function and an analytical and physical explanation which remarkably reproduces the asymptotic scaling exponent of -4 .

Now, we discuss what happens if the disorder increases further. In Fig. 1(b), we increase the disorder strength and study the WQTI-AI transition. For $G \gtrsim 0.3$, the scaling flow is to 1 with the rate being progressively faster for larger (closer to 1) G . On the contrary, when the disorder is strong enough, the conductance is suppressed close to zero, and more importantly, does not depend on the system size. This change of scaling marks the WQTI-AI phase transition. The small finite conductance in the AI phase might be caused by rare conducting bubbles. These bubbles are incoherent, so the finite-size scaling law should obey the Ohmic law, i.e., L^0 for 2D, albeit the conductance magnitude is much smaller than the conductance quantum because of strong localization with $G \sim 0$. Combining with the previous argument, the scaling exponent β is negative for $G > G_c \sim 0.3$ and approaches -4 in the limit $G \rightarrow 1$; for $G < G_c$, $\beta = 0$ [45]. We note one difference with the transverse conductance measurement in which $\beta < 0 (> 0)$ for $G > 0.5 (< 0.5)$ and there is only one fixed point ($\beta = 0$) at $G = 0.5$ [40]. The reason for this disparity is that the rare conducting bubbles support longitudinal but not transverse conductivity.

While the TI-WQTI boundary can be obtained analytically from $\text{Im} \Sigma_0$, it is not so obvious for the WQTI-AI transition because of very strong disorder. Instead, we look at where our self-energy approximation breaks down and the Anderson localization physics prevails. The hybridization probability already shows that the factor $\Gamma/\Delta E$, if being large, can significantly couple the two edges and can completely suppress the edge conductance. Since the hybridization can happen through either the upper or lower bulk bands, we propose a

quantity to capture its magnitude,

$$\Xi = \frac{\text{Im } \Sigma_0}{\bar{\mu} + |\bar{m}|} + \frac{\text{Im } \Sigma_0}{|\bar{m}| - \bar{\mu}}. \quad (2)$$

The physical driving mechanism of the WQTI-AI transition is the disorder-induced density of percolating states inside the energy gap, which can be estimated by $\rho(\mu) \sim \text{Im } \Sigma_0 / (\bar{m}^2 - \bar{\mu}^2)$. This shows that Eq. (2) is indeed consistent with the microscopic physics. Therefore, we expect the Ξ function including the imaginary part of the self-energy to resolve the inconsistency between the renormalized energy gap (obtained from only the real part of the self-energy) and the numerically generated conductance. In particular, by fixing Ξ to a constant, we can reproduce the boundary of the numerical quantization regime. To verify this, we apply our theory to explain the dependence of the TAI phase on the correlation length of the disorder. This effect has been studied in a few papers [43,44], based mostly on numerical simulations.

III. NUMERICAL PHASE DIAGRAM

A. $m > 0$

We first study the case where the clean limit is a nontrivial TI, i.e., for $W = 0$, the longitudinal conductance is quantized for $m < \mu < -m$. To connect with our finite-size simulation, we identify the region of G within 10% error from unity as the quantization plateau, rather than the critical value 0.3 derived earlier from the scaling analysis. The first remark is that while the renormalized energy gaps (black lines) are clearly larger than the quantization regime, the isolines $\Xi = 2$ (purple lines) consistently enclose this region, even as ξ changes. These results also agree with the absence of quantization plateau in the $\mu < m$ region, despite still being within the energy gap. This is strong validation of the theory.

We now focus on the fate of the TAI in the presence of long-range correlated disorder. Although a prominent TAI region, i.e., the part of the quantization plateau with $\mu > -m$, is visible for $\xi = 2$ [Fig. 2(a)], it is suppressed quickly with longer correlation lengths [Figs. 2(b) and 2(c)]. The trend appears more apparent in Fig. 2(d) where we collect all the Ξ isolines for different correlation lengths. The naive explanation is that the exponential suppression induced by ξ prevents the energy gap to broaden [45], thus ruling out the TAI. This limit is approximately reached for $\xi = 20$, indicated by the almost symmetry around $\mu = 0$. However, the TAI already vanishes for $\xi = 8$ despite a visibly widened energy gap. In fact, we show that the ξ dependence is mostly due to the rapid increase of $\text{Im } \Sigma_0$ passing the critical point, rather than the decrease of the gap [45].

B. $m < 0$

We now consider the case where disorder inverts the sign of the mass, thus introducing nontrivial topology to an otherwise trivial system. By definition, the whole quantization plateau is now TAI. As can be seen from Figs. 3(a)–3(c), the TAI phase is suppressed for long-ranged disorder, similar to the case of $m < 0$. Again, the naive argument predicts that the TAI should disappear when a sufficiently long correlation length suppresses the mass inversion by rendering the quadratic

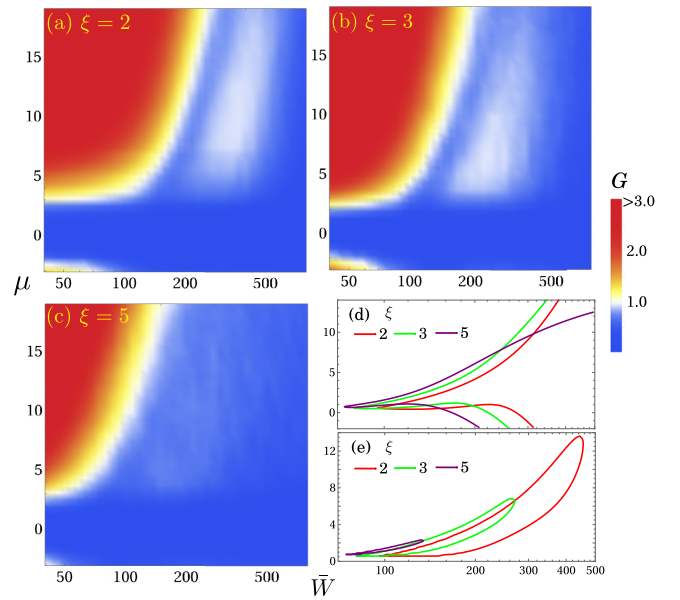


FIG. 3. (a)–(c) Numerical simulations for the trivial clean limit. The width is $350a$, the length is $700a$, $m = 1$, $\alpha = 120$, $\beta = 400$, $\gamma = 200$. (d) The renormalized energy gaps for different disorder correlation lengths corresponding to (a)–(c). (e) Similar to (d) but for the $\Xi = 2$ isolines.

terms in the Hamiltonian irrelevant [20,21,30]. However, our numerical simulations show a complete loss of quantization even at a moderate $\xi = 5$ where the mass inversion is still clearly present. On the other hand, the isoline $\Xi = 2$ exhibits a consistent shrinkage of the TAI phase. We note that the quantitative agreement here between the theoretical and numerical results is not as good as the $m < 0$ case. The reason might be that the mass first needs to be inverted so the TAI plateau now exists at a very high disorder strength. Our analytical theory only includes noncrossing diagrams [45], so we expect its accuracy to degrade at very strong disorder. Nevertheless, theoretical and numerical results in Fig. 3 show similar trends. These two examples demonstrate that our theory, particularly the Ξ function, is an effective tool to study the disorder-driven topology.

IV. CONCLUSION

We theoretically identify several different class A disordered 2D TI phases, including TI (perturbatively weak disorder), WQTI (moderate disorder), and AI (strong disorder). Our analytical theory, directly supported by numerical simulations, relies on the imaginary part of the disorder-induced self-energy, which was ignored in earlier studies. One might raise a question about the extremely accurate quantization in integer quantum Hall experiments. In addition to various quantitative reasons, e.g., large gap, a protective mechanism is based on the bulk of a Hall insulator being localized at essentially all energy. This is because the Landau levels are exactly flat, and in the presence of disorder, quickly collapse into localized states (except when the sample is very small). The WQTI mechanism is not possible because it requires extended bands around the energy gap.

In earlier works [20,21], the disorder is uncorrelated and zero ranged, and the TAI is predicted to be a generic phase. However, our analysis with nonzero correlation lengths shows that TAI is fragile and vanishes for long-range disorders. In 2D semiconductors [8–10], the dominant disorder is always the long-range correlated Coulomb disorder arising from random quenched charge impurities [49,50], and hence the TAI phase is difficult to observe [except perhaps in artificial atomic, molecular, and optical systems [34,39]]. Our work establishes TI, WQTI, and AI as the three generic phases in the presence of disorder, with WQTI being a somewhat fragile intermediate critical phase in between the weak-disorder TI and the strong-disorder AI phase.

Lastly, we compare our “weak quantization” with the “quantization loss” due to intraedge coupling between the two spin sectors in quantum spin Hall insulators [51,52]. Being a local process, the latter cause a finite deviation from the quantized conductance even in the thermodynamic while in our model the quantization recovers slowly. Moreover, the intraedge backscattering is not possible in noninteracting systems.

ACKNOWLEDGMENTS

This work is supported by and Laboratory for Physical Sciences. This work is also generously supported by the High Performance Computing Center (HPCC) at the University of Maryland.

-
- [1] D. J. Thouless, M. Kohmoto, M. P. Nightingale, and M. den Nijs, *Phys. Rev. Lett.* **49**, 405 (1982).
- [2] M. Kohmoto, *Ann. Phys.* **160**, 343 (1985).
- [3] F. D. M. Haldane, *Phys. Rev. Lett.* **61**, 2015 (1988).
- [4] M. Z. Hasan and C. L. Kane, *Rev. Mod. Phys.* **82**, 3045 (2010).
- [5] X.-L. Qi and S.-C. Zhang, *Rev. Mod. Phys.* **83**, 1057 (2011).
- [6] B. A. Bernevig, *Topological Insulators and Topological Superconductors* (Princeton University Press, Princeton, NJ, 2013).
- [7] T. D. Stanescu, *Introduction to Topological Quantum Matter and Quantum Computation* (Taylor and Francis, London, 2016).
- [8] C. L. Kane and E. J. Mele, *Phys. Rev. Lett.* **95**, 226801 (2005).
- [9] B. A. Bernevig, T. L. Hughes, and S. C. Zhang, *Science* **314**, 1757 (2006).
- [10] C. Liu, T. L. Hughes, X.-L. Qi, K. Wang, and S.-C. Zhang, *Phys. Rev. Lett.* **100**, 236601 (2008).
- [11] M. König, S. Wiedmann, C. Brüne, A. Roth, H. Buhmann, L. W. Molenkamp, X.-L. Qi, and S.-C. Zhang, *Science* **318**, 766 (2007).
- [12] A. Roth, C. Brüne, H. Buhmann, L. W. Molenkamp, J. Maciejko, X.-L. Qi, and S.-C. Zhang, *Science* **325**, 294 (2009).
- [13] I. Knez, R.-R. Du, and G. Sullivan, *Phys. Rev. Lett.* **107**, 136603 (2011).
- [14] R. Yu, W. Zhang, H.-J. Zhang, S.-C. Zhang, X. Dai, and Z. Fang, *Science* **329**, 61 (2010).
- [15] C.-Z. Chang, J. Zhang, X. Feng, J. Shen, Z. Zhang, M. Guo, K. Li, Y. Ou, P. Wei, L.-L. Wang *et al.*, *Science* **340**, 167 (2013).
- [16] C.-Z. Chang, W. Zhao, J. Li, J. K. Jain, C. Liu, J. S. Moodera, and M. H. W. Chan, *Phys. Rev. Lett.* **117**, 126802 (2016).
- [17] M. Büttiker, *Phys. Rev. B* **38**, 9375 (1988).
- [18] R. Shindou and S. Murakami, *Phys. Rev. B* **79**, 045321 (2009).
- [19] S. Ryu and K. Nomura, *Phys. Rev. B* **85**, 155138 (2012).
- [20] C. W. Groth, M. Wimmer, A. R. Akhmerov, J. Tworzydło, and C. W. J. Beenakker, *Phys. Rev. Lett.* **103**, 196805 (2009).
- [21] J. Li, R. L. Chu, J. K. Jain, and S. Q. Shen, *Phys. Rev. Lett.* **102**, 136806 (2009).
- [22] H. Jiang, L. Wang, Q.-f. Sun, and X. C. Xie, *Phys. Rev. B* **80**, 165316 (2009).
- [23] L. Fu and C. L. Kane, *Phys. Rev. Lett.* **109**, 246605 (2012).
- [24] D. Xu, J. Qi, J. Liu, V. Sacksteder, X. C. Xie, and H. Jiang, *Phys. Rev. B* **85**, 195140 (2012).
- [25] J. Song, H. Liu, H. Jiang, Q.-f. Sun, and X. C. Xie, *Phys. Rev. B* **85**, 195125 (2012).
- [26] J. Song and E. Prodan, *Phys. Rev. B* **89**, 224203 (2014).
- [27] W. Qin, D. Xiao, K. Chang, S.-Q. Shen, and Z. Zhang, *Sci. Rep.* **6**, 39188 (2016).
- [28] C. Liu, W. Gao, B. Yang, and S. Zhang, *Phys. Rev. Lett.* **119**, 183901 (2017).
- [29] H. Huang and F. Liu, *Phys. Rev. B* **98**, 125130 (2018).
- [30] S. S. Krishtopenko, M. Antezza, and F. Tepepe, *Phys. Rev. B* **101**, 205424 (2020).
- [31] C.-B. Hua, Z.-R. Liu, T. Peng, R. Chen, D.-H. Xu, and B. Zhou, *Phys. Rev. B* **104**, 155304 (2021).
- [32] A. Haim, R. Ilan, and J. Alicea, *Phys. Rev. Lett.* **123**, 046801 (2019).
- [33] W. Li, J. Zang, and Y. Jiang, *Phys. Rev. B* **84**, 033409 (2011).
- [34] G.-G. Liu, Y. Yang, X. Ren, H. Xue, X. Lin, Y.-H. Hu, H.-x. Sun, B. Peng, P. Zhou, Y. Chong, and B. Zhang, *Phys. Rev. Lett.* **125**, 133603 (2020).
- [35] A. Altland, D. Bagrets, L. Fritz, A. Kamenev, and H. Schmiedt, *Phys. Rev. Lett.* **112**, 206602 (2014).
- [36] I. Mondragon-Shem, T. L. Hughes, J. Song, and E. Prodan, *Phys. Rev. Lett.* **113**, 046802 (2014).
- [37] S. Velury, B. Bradlyn, and T. L. Hughes, *Phys. Rev. B* **103**, 024205 (2021).
- [38] L. Lin, Y. Ke, and C. Lee, *Phys. Rev. B* **103**, 224208 (2021).
- [39] E. J. Meier, F. A. An, A. Dauphin, M. Maffei, P. Massignan, T. L. Hughes, and B. Gadway, *Science* **362**, 929 (2018).
- [40] M. Onoda and N. Nagaosa, *Phys. Rev. Lett.* **90**, 206601 (2003).
- [41] M. Onoda, Y. Avishai, and N. Nagaosa, *Phys. Rev. Lett.* **98**, 076802 (2007).
- [42] Y. Y. Zhang and S. Q. Shen, *Phys. Rev. B* **88**, 195145 (2013).
- [43] A. Girschik, F. Libisch, and S. Rotter, *Phys. Rev. B* **88**, 014201 (2013).
- [44] A. Girschik, F. Libisch, and S. Rotter, *Phys. Rev. B* **91**, 214204 (2015).

- [45] See Supplemental Material at <http://link.aps.org/supplemental/10.1103/PhysRevB.106.134201> for long-range correlated disorder and the self-consistent Born approximation and additional numerical data.
- [46] R. Landauer, *Philos. Mag.* **21**, 863 (1970).
- [47] C. W. Groth, M. Wimmer, A. R. Akhmerov, and X. Waintal, *New J. Phys.* **16**, 063065 (2014).
- [48] L. Chen, Q. Liu, X. Lin, X. Zhang, and X. Jiang, *New J. Phys.* **14**, 043028 (2012).
- [49] J. D. Watson, S. Mondal, G. A. Csáthy, M. J. Manfra, E. H. Hwang, S. Das Sarma, L. N. Pfeiffer, and K. W. West, *Phys. Rev. B* **83**, 241305(R) (2011).
- [50] S. Das Sarma, E. H. Hwang, S. Kodiyalam, L. N. Pfeiffer, and K. W. West, *Phys. Rev. B* **91**, 205304 (2015).
- [51] T. L. Schmidt, S. Rachel, F. von Oppen, and L. I. Glazman, *Phys. Rev. Lett.* **108**, 156402 (2012).
- [52] J. I. Väyrynen, M. Goldstein, and L. I. Glazman, *Phys. Rev. Lett.* **110**, 216402 (2013).